MSense: boosting wireless sensing capability under motion interference

Zhaoxin Chang, Fusang Zhang, Jie Xiong, Weiyan Chen, Daqing Zhang

MSense: Boosting Wireless Sensing Capability Under Motion Interference

Zhaoxin Chang[1], Fusang Zhang[2], Jie Xiong[3], Weiyan Chen[4], Daqing Zhang[1,5]
[1]SAMOVAR, Telecom SudParis, Institut Polytechnique de Paris,
[2]Institute of Software, Chinese Academy of Sciences and University of Chinese Academy of Sciences,
[3]Microsoft Research Asia and University of Massachusetts Amherst,
[4]China Mobile Research Institute, [5]Peking University

ABSTRACT

Wireless signals have been widely utilized for human sensing. However, wireless sensing systems face a fundamental limitation, i.e., the wireless device must keep static during the sensing process. Also, when sensing fine-grained human motions such as respiration, the human target is required to stay stationary. This is because wireless sensing relies on signal variations for sensing. When device is moving or human body is moving, the signal variation caused by the target area (e.g., chest for respiration sensing) is mixed with the signal variation induced by device or other body parts, failing wireless sensing. In this paper, we propose MSense, a general solution to deal with motion interference from wireless device and/or human body, moving wireless sensing one step forward towards real-life adoption. We establish the sensing model by taking both device motion and interfering body motion into consideration. By extracting the effect of body and device motions through pure signal processing, the motion interference can be removed to achieve accurate target sensing. Comprehensive experiments demonstrate the effectiveness of the proposed scheme. The achieved solution is general and can be applied to different sensing tasks involving both periodic and aperiodic motions.

CCS CONCEPTS

• **Human-centered computing** → **Ubiquitous and mobile computing systems and tools**.

KEYWORDS

Wireless sensing, Motion interference cancellation, Body motion and device motion interference, MmWave radar

1 INTRODUCTION

Wireless signals have demonstrated their sensing capabilities in many applications including vital sign monitoring [21, 41], gesture recognition [26, 46], activity sensing [27, 61], tracking [6, 35], vibration detection [23, 57], and material identification [8, 47]. In recent years, various types of wireless signals have been utilized for sensing purposes, including Wi-Fi [34, 50], RFID [53, 66], LoRa [62, 64], UWB [16, 48], LTE [13, 18], mmWave [49, 58] and acoustic signals [37, 39].

Corresponding Authors: Daqing Zhang and Fusang Zhang.

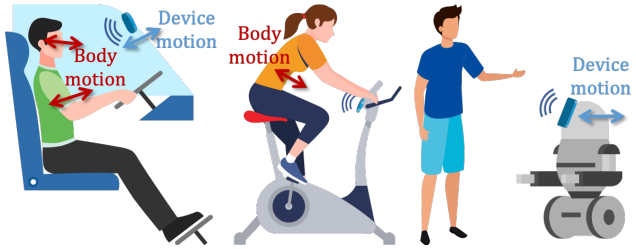

Figure 1: Scenarios of wireless sensing under device and/or body motion: (a) Eye blinking detection in a moving car. (b) Respiration monitoring during exercise. (c) Gesture recognition using robot-carried device.

Although wireless sensing has achieved promising progress, wireless sensing still faces a fundamental limitation, i.e., it works under stationary conditions. Take respiration sensing as an example. The human target is required to stay stationary for sensing. If the target is running on a treadmill or walking, it is very difficult to extract the respiration information. During the sensing process, the wireless device used for sensing also needs to be stationary. If we place the device on a moving robot or hold it in hand with just small involuntary motions, the sensing performance severely degrades. This is because the underlying principle behind wireless sensing is that target motions can influence signal propagation, causing signal variations at the receiver. By analyzing the signal variations, target motion information can be inferred. However, when device is moving or/and the human body is moving, the signal variations caused by these interference motions are mixed with the signal variations caused by the target area (e.g., chest for respiration), failing wireless sensing. In real life, we do have a lot of scenarios with device motions or/and body motions. For example, as shown in Figure 1a, when we try to sense the driver's eye blinks for fatigue driving detection, the car movements bring motions to both device and human body. Similarly, as shown in Figure 1b, when monitoring vital signs during exercise,

the whole body moves dramatically, inducing strong motion interference. When we place the sensing device on a moving robot for sensing as shown in Figure 1c, the device motion also causes severe interference. These large motion interference can easily bury the small variations induced by target (e.g., eye blink and respiration).

To address the device motion, a recent work [65] proposed to adopt a static object such as a wall in the surrounding environment as a reference to cancel out the effect of device motion. Although efficient, this method only works with periodic target motions. Furthermore, this method could not be applied to address body motions. Several approaches [15, 20, 55, 71] were proposed to deal with interference from human body leveraging deep learning methods. However, even with deep learning, these methods still only work with periodic target motions (e.g., vital sign monitoring). The underlying principle is that the periodicity of the target motions differs dramatically from that of the body movements. However, many real-world applications involve aperiodic motions such as hand gestures. Furthermore, even for respiration which is usually periodic, people are more interested in those abnormal part (e.g., apenea) which is aperiodic. In scenarios with motion interference from both human body and device (e.g., sensing in a moving car), the problem becomes even more challenging.

In this paper, we propose MSense, a general solution to deal with motion interference induced by human motions and device motions in wireless sensing. For the first time, we model the effect of target motions together with device and body motions. First of all, we find that the signal received at the receiver may contain signals reflected from different body parts. For mmWave radar with a bandwidth of 4 GHz, the range bin resolution is around 5 cm, which is capable of separating signal reflected from the head and signal reflected from the leg into two different bins. However, the signal reflected from the eye and the signal reflected from the mouth have a path length difference smaller than the range bin resolution and therefore they fall in the same bin. In this case, the two signals can not be separated in the time domain. We therefore further utilize the antenna array widely available at the commodity mmWave hardware to separate signals in the spatial domain.

After we obtain the signal reflected just from the target area (e.g., eye area for blink detection), this signal contains not just the information of target motion but also the information of body motion (interference) and device motion (interference). To address this challenge, we leverage one observation: while the reflection signal from the target area carries the information of target, body motion and device motion, some reflection signals from other body parts may contain just the information of body motion and device motion. In this case, the undesired motion interference can be canceled out to obtain clean target motion information. However, we also notice that signals reflected from different body areas can contain distinct body motions. Therefore, we need to select an area with the same body and device motions as the target area for interference motion cancellation. For example, for eye blink detection, the forehead-reflected signal contains motion information of head and device. The eye-reflected signal contains motion information of head, device, and eye (i.e., target). These two signals can be used for interference motion cancellation. On the other hand, a signal reflected from the neck which contains motion information of neck and device can not be used for cancellation. To select the most appropriate reflection signal for cancellation, we maximize an objective function based on the known clean signal pattern (e.g., eye blink-induced signal variations contain sparse short pulses in time domain). Note that this solution is independent of the periodicity of the target motion.

We implement MSense using a commodity mmWave radar (TI IWR1843BOOST). We conduct comprehensive experiments to validate the effectiveness of the proposed approach. We employ three representative applications to evaluate the sensing performance: i) in-vehicle eye blink, yawn, and nod detection (i.e., with both body and device motion interference); ii) respiration monitoring during exercise (i.e., with just body motion interference); and iii) hand gesture recognition when the mmWave device is placed on a moving robot (i.e., with just device motion interference). For all three applications, our system achieves highly accurate sensing. The main contributions of this work are summarized as follows.

- We address one important practical challenge, i.e., device and body motion interference in wireless sensing in this work. We believe this is one critical step toward real-life adoption of wireless sensing.
- We propose a signal processing scheme to remove body and device motion interference without a need of training or learning.
- We implement MSense and comprehensively evaluate its performance. We employ three representative sensing tasks to demonstrate the effectiveness and generalization of our system. Experiments show that our approach can be applied to sense both periodic and aperiodic motions.

2 PRELIMINARY

In this section, we first present the background knowledge of mmWave radar signals and then introduce the traditional sensing scheme under static conditions.

2.1 MmWave Radar Primer

MmWave radar refers to radar that operates in the millimeter wave frequency band. As shown in Figure 2a, mmWave

radar transmits signals to the environment. Then, part of the signals are reflected by static objects and the human target. By capturing the reflected mmWave signals, the range, velocity, and angle of each object can be estimated. Currently, frequency-modulated continuous wave (FMCW) technology is typically used by mmWave radars for signal modulation, utilizing chirp as the basic signal unit. The transmitted chirp signal can be represented as:

$$S_T(t) = A_T \cos 2\pi (f_c t + \frac{1}{2} k t^2), \tag{1}$$

where A_T, f_c, and k are the amplitude, starting frequency, and chirp slope, respectively. The transmitted chirp propagates in the environment and then is reflected back to the radar by the objects. Because the distances from each object to the radar are different, the propagation path lengths and time delays of the reflected signals from each object are different. Therefore, the received signal is composed of multiple copies of the transmitted chirp with different delays and attenuation. After capturing the received signal, FMCW radar mixes it with the transmitted chirp and employs a low-pass filter to obtain the intermediate frequency (IF) signal denoted by:

$$S(t) = \sum_{n=1}^{N} A_n \cos\left(2\pi \frac{2kR_n}{c} t + \frac{4\pi f_c R_n}{c}\right), \tag{2}$$

where N, A_n, R_n, and c are the number of objects that reflect signal, the amplitude of n-th object-reflected signal, the distance of n-th object, and the speed of light, respectively. It can be seen that the IF signal of FMCW radar is composed of multiple cosine components. Each cosine signal corresponds to an object's reflection signal, and its frequency ($\frac{2kR_n}{c}$) is determined by the distance of the object from the radar. The amplitude and phase of each frequency component contained in the IF signal can be obtained by performing Fast Fourier Transform (FFT) on the IF signal, which can generate several frequency bins. According to Equation 2, if there is an object reflecting signal at a distance of R_n, after performing FFT on the IF signal, the bin with a frequency of $f = \frac{2kR_n}{c}$ shows a high magnitude peak. Therefore, by observing the frequency spectrum obtained after performing FFT on the IF signal, we can estimate at which distances objects exist. This operation of estimating the target distance is called Range-FFT. The frequency bin in the FFT result is denoted as range bin. Performing Range-FFT on each chirp can obtain the range estimation results at different moments to obtain the range profile.

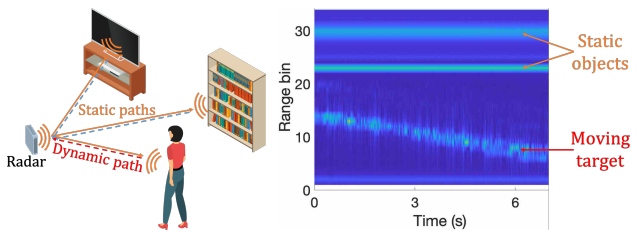

(a) Sensing scenario. (b) Range profile.

Figure 2: MmWave radar-based sensing primer.

Figure 2b shows an example of the range profile. When the movement of an object (i.e., human walking) is large enough to cause the distance to change significantly (i.e., the range bin where the object is located changes), the movement of the object can be tracked on the range profile. On the contrary, subtle target motion (e.g., respiration) may be not enough to cause the change of its range bin, making it cannot be observed directly on the range profile. Fortunately, subtle motion can be estimated by extracting the phase change of the range bin where the target is located over time, providing more fine-grained sensing granularity than only measuring range bin change. Note that the phase of a range bin can be directly extracted from the result of Range-FFT. According to Equation 2, the Range-FFT result of the range bin where the object with distance R_n is located can be represented as:

$$y_n(t) = A_n e^{j\frac{4\pi f_c}{c} R_n(t)} = A_n e^{jKR_n(t)}, \tag{3}$$

and the phase can be extracted as: $\varphi(t) = KR_n(t) = \frac{4\pi f_c}{c} R_n(t)$. Then, the displacement of the object can be calculated as $\Delta R_n = \frac{c}{4\pi f_c} \Delta\varphi$. For instance, target motion with a displacement of 1 mm can induce a phase change of 1.03π ($f_c = 77$ GHz). Thus, phase information extraction is the basis for fine-grained sensing tasks.

2.2 Sensing Under Static Conditions

In this section, we present the basis of traditional fine-grained sensing using body reflection signals under static conditions. As shown in Figure 3a, a radar emits signals and receives signals reflected from various body areas. Since the distance from each body area to the radar is different, the reflected signal of the human body will appear on multiple range bins. However, reflected signals from different body areas with similar distances to the radar may lie within one range bin and thus cannot be distinguished. Specifically, two areas cannot be distinguished when the distance difference between them is smaller than the *range resolution*. The range resolution of the mmWave radar is determined by the bandwidth of the chirp signal, which is $R_{res} = \frac{c}{2B}$, where B is the bandwidth [5]. Due to this limited range resolution, reflected signals from body areas with a similar distance to the radar will be in the same range bin and mixed. In the case shown in Figure 3a, chest, abdomen, and leg areas are in the same range bin #4.

Here, we first present the model of body-reflected signal without device and body motion. Assume that the person

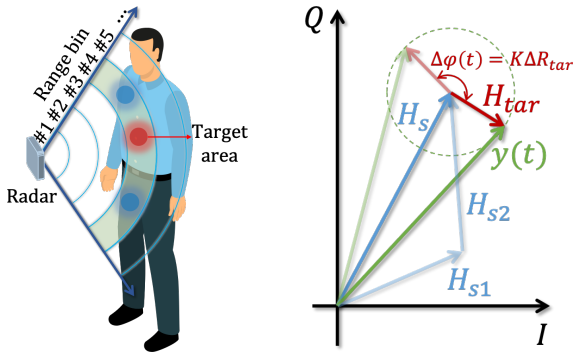

(a) Illustration of body reflections. **(b) Signal in range bin #4 on I-Q plane.**

Figure 3: Sensing based on body reflection under static conditions.

in Figure 3a has no movement other than breathing. Within range bin #4, chest and abdomen areas have displacement induced by respiration, which is the target motion to sense. Meanwhile, other areas (i.e., the area between neck and chest, and leg area) keep static. Therefore, based on Equation 3, the reflected signal in range bin #4 is a composition of multi-area reflected signals:

$$\begin{aligned} y(t) &= \sum_{p=1}^{P} A_p e^{jKR_p(t)} \\ &= \sum_{p\in P_s} A_p e^{jKR_{p0}} + \sum_{p\in P_d} A_p e^{jKR_{p0}} e^{jK\Delta R_{tar}(t)} \\ &= H_s + H_{tar} e^{jK\Delta R_{tar}(t)}, \end{aligned} \tag{4}$$

where P, P_s, and P_d are the set of all points, static points, and dynamic points respectively. A_p, R_{p0}, and $\Delta R_{tar}(t)$ are the amplitude of the p-th point-reflected signal, the initial distance of the p-th point, and the breath-induced displacement (target motion) over time. The points in an area can be represented as one vector due to the same motion pattern. As shown in Figure 3b, the signal in range bin #4 is a superposition of two static vectors H_{s1} and H_{s2}, which represent the signals reflected from two static areas, and a dynamic vector $H_{tar}e^{jK\Delta R_{tar}(t)}$ on the I-Q plane. Two static vectors mix together as one static vector H_s. The dynamic vector rotates with respect to the static vector. As a result, the phase of the composite signal $y(t)$ also changes with respiration motion. Therefore, by extracting the phase change of the composite signal, the breath waveform can be restored.

3 PRINCIPLE OF BODY AND DEVICE MOTIONS ELIMINATION

In this section, we first present the body-reflection model under body and device motion. Then, we propose a model-based approach to eliminate the effect of body and device motions on the target sensing task.

3.1 Modeling Body and Device Motion Interference

In this section, we involve body and device motion in the body reflection model presented in Section 2.2. We use eye-blinking detection in a moving car as an example to analyze the effect of body and device motion on target sensing. When the human body and device are static, the closing and opening of the eyelids caused by blinking can induce a subtle phase change in eye-reflected signal. Thus, by monitoring the phase change of eye-reflected signal, blinking can be detected [22]. In a mobile scenario (i.e., a moving car), due to the car's bump, the human body also has body motion. Meanwhile, the device also vibrates with the car. For now, all signal propagation path lengths change with body and device motion. Figure 4 illustrates the path length variation under body and device motions. For target area (i.e., eye area in this example), in addition to target motion ($\Delta R_{tar}(t)$), target area also exhibits irrelevant body motion ($\Delta R_{body,tar}(t)$). On the other hand, device motion ($\Delta d_{dev}(t)$) causes target area reflected path length to change ($\Delta R_{dev,tar}(t)$). Therefore, the change of target area reflected path length is $\Delta R_{tar}(t)+\Delta R_{body,tar}(t)+\Delta R_{dev,tar}(t)$. Similarly, the path length change of a non-target area is $\Delta R_{body,m}(t)+\Delta R_{dev,m}(t)$, where $\Delta R_{body,m}(t)$ and $\Delta R_{dev,m}(t)$ are the body motion and device motion induced path length change for the m-th area, respectively. To this end, the signal of the range bin (Equation 4) with human target should be

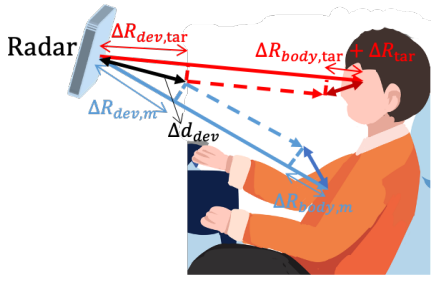

Figure 4: Illustration of the effect of body and device motion on signals reflected from different body areas.

modified as:

$$y'(t) = H_{tar} e^{jK(\Delta R_{tar}(t)+\Delta R_{body,tar}(t)+\Delta R_{dev,tar}(t))} + \sum_{m=1}^{M} H_m e^{jK(\Delta R_{body,m}(t)+\Delta R_{dev,m}(t))}, \quad (5)$$

where M is the number of areas without target motion. Therefore, due to the existence of body and device motions, there is no static component in the body reflection signal. Static vectors in the model under static condition (in Section 2.2) also become dynamic vectors. It can be seen from Equation 5 that there are two terms of interference that prevent us from extracting motion information ($\Delta R_{tar}(t)$) related to the sensing target task using traditional approaches: i) the random body and device motions ($\Delta R_{body,tar}(t) + \Delta R_{dev,tar}(t)$) in the sensing target area; ii) the motions of other body areas ($\sum_{m=1}^{M} H_m e^{jK(\Delta R_{body,m}(t)+\Delta R_{dev,m}(t))}$) is superimposed with the target area reflected signal. Note that different body areas can have distinct movement patterns. For example, the head can nod and shake, so it can have different movement patterns from the chest during the bumping of the car. Thus, the range bin where the target area is located may be superimposed with signals from other areas with different body motion patterns. On the other hand, since device motion causes the length of each signal reflection path to change simultaneously, the signal variation patterns caused by device motion in the reflected signals of different body areas are similar.

Figure 5 shows the interference of body and device motion on eye blink detection and respiration monitoring. For both sensing tasks, we first collect signals in static conditions, i.e., the device and body keep stationary during the sensing process. For eye blink detection, millimeter-scale phase changes caused by five blinks can be clearly identified. For respiration monitoring, periodic movements induced by inhalation and exhalation can be observed. However, when repeating the experiment in a moving car, due to the body and device motions caused by the bumping of the car, the head-reflected signal exhibits a random phase fluctuation on a larger scale shown in Figure 5a, thereby failing the eye blink detection. As shown in Figure 5b, the same phenomenon can be observed when monitoring the breathing of an exercising person.

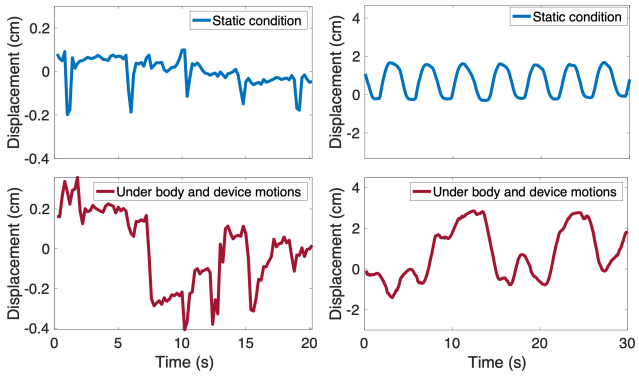

(a) Eye blink detection. (b) Respiration monitoring.

Figure 5: Comparison of signals in static condition with signals under body and device motions.

3.2 Body and Device Motion Elimination

In this section, we propose a two-stage strategy to eliminate the effect of body and device motion on sensing. Specifically, we first extract the reflected signals from the target area from the superimposed received signal. This allows us to focus on processing reflections from just the target area and avoid potential interference from other areas with different motion patterns. After obtaining the signal reflected just from the target area, we further eliminate the information of body and device motion to recover the target motion.

To extract the target area reflected signal from the raw signal, we leverage one observation, which is *in the view of radar, the angles of different body areas are different.* Note that antenna array is widely available on commodity mmWave radar, we thus propose to use digital beamforming with signals received by multiple antennas to enhance the reflected signals from the target area. As shown in Figure 6, the angles of the target area (e.g., eye) and another area (e.g., chest) are θ_{tar} and θ_m, respectively. Then, based on Equation 3, the phase difference between adjacent antennas induced by the reflection signals from these two areas are $\Delta\varphi_{tar} = Kd\sin\theta_{tar}$ and $\Delta\varphi_m = Kd\sin\theta_m$ respectively. Figure 6 illustrates the vectors of H_{tar} and H_m of different antennas on I-Q plane. To enhance the reflected signal from target area at angle θ_{tar}, we multiply the signal of the i-th antenna by the factor $e^{-j(i-1)\Delta\varphi_{tar}} = e^{-j(i-1)Kd\sin\theta_{tar}}$. Then, H_{tar} on all antennas have the same phase on I-Q plane now, while H_m on different antennas still have a phase difference. We add the signals of each antenna after multiplying the factors. Consequently, after adding up H_{tar} of all antennas, a vector with a larger magnitude is generated. On the contrary, because the phases of H_m are not aligned, the magnitude of the vector formed after adding up is much smaller than that of H_{tar}. In this way, the reflected signal from the target area at an angle of θ_{tar} is enhanced. The interfering reflected signals from other body areas in different directions are weakened. Thus, we obtain the target area reflected signal using digital beamforming, which can be expressed as:

$$y_{tar}(t) = H_{tar} e^{jK(\Delta R_{tar}(t)+\Delta R_{body,tar}(t)+\Delta R_{dev,tar}(t))}. \quad (6)$$

Note that the more antennas used for beamforming, the better the enhancement effect on reflected signals from target area [54].

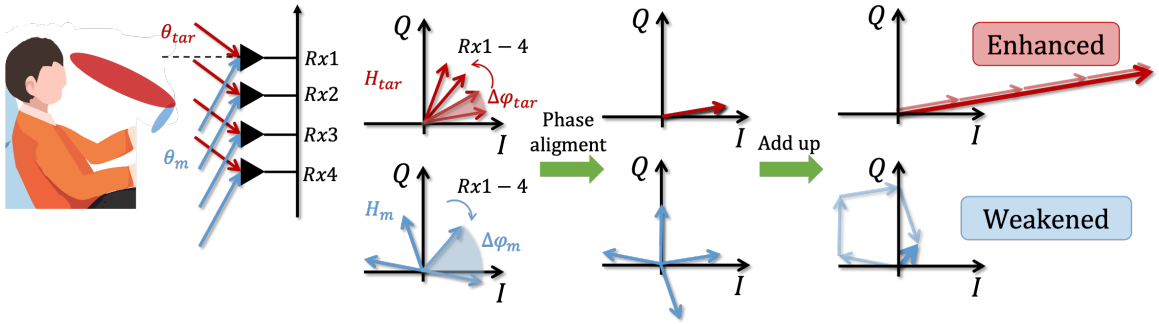

Figure 6: Illustration of beamforming the received signal at a specific direction.

For now, we still need to eliminate the interference of body and device motions ($\Delta R_{body,tar}(t) + \Delta R_{dev,tar}(t)$) in the target area reflected signal to recover target motion ($\Delta R_{tar}(t)$). *Our core observation is that non-target area reflected signals may contain just the information of body and device motion.* Intuitively, if we can first estimate the device motion and body motion by extracting the reflected signal from another area, these undesired motion interference can be further eliminated from the target area reflected signal. It is worth noting that we need to carefully select an area where body and device motions are the same as the target area for estimation. Fortunately, such areas are usually available, because two adjacent body areas have the same body and device motions. As the example shown in Figure 7, in a moving car, eye-reflected signal and forehead-reflected signal contain the same body and device motions. On the contrary, the chest area has different body motion from the eye area, because the head usually has more complex movement patterns compared with the chest. Meanwhile, due to the large difference in the angle of the chest and eyes relative to the radar, the values of phase change due to device motion in the signal reflected from chest area and from eye area are also different [65]. Thus, the forehead-reflected signal can be utilized for device and body motion estimation in eye blink detection. Then, device and body motion interference can be eliminated from the eye-reflected signal, enabling eye blink detection in the moving car.

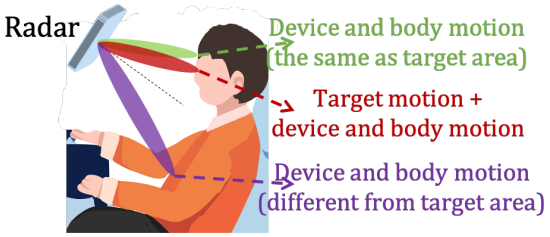

Figure 7: Body and device motion elimination. The area adjacent to the target area may exhibit the same device and body motion as target area, which can be used for motion elimination.

To realize our idea, the key is to obtain the reflection signal of an area, which has the same body and device motion as the target area. To achieve this, we still utilize the beamforming approach. By beamforming the signal to the area near the target area, we can obtain a signal that only contains the same body and device motions as the target area:

$$y_0(t) = H_0 e^{jK(\Delta R_{body,tar}(t)+\Delta R_{dev,tar}(t))}. \tag{7}$$

Then, we propose to eliminate the effect of body and device motions in target area through a division operation between the target area reflection signal and the adjacent area reflection signal:

$$\begin{aligned} y_{new}(t) = \frac{y_{tar}(t)}{y_0(t)} &= \frac{H_{tar}}{H_0} \frac{e^{jK(\Delta R_{tar}(t)+\Delta R_{body,tar}(t)+\Delta R_{dev,tar}(t))}}{e^{jK(\Delta R_{body,tar}(t)+\Delta R_{dev,tar}(t))}} \\ &= H_{new} e^{jK\Delta R_{tar}(t)}. \end{aligned} \tag{8}$$

By extracting the phase of $y_{new}(t)$, the target motion information $\Delta R_{tar}(t)$ can be obtained.

4 MSENSE DESIGN

In this section, we present the detailed design of our system. As illustrated in Figure 8, our system consists of three key modules: signal preprocessing, candidate signal extraction, and motion elimination. Briefly, we first detect in which range bins human body is located. Subsequently, for each of these identified range bins, we leverage MVDR algorithm to estimate the angles associated with the reflections from various areas of the body. By beamforming the received signal to these angles, we extract potential candidate signals. To cancel out the effect of body and device motion interference, we pair up the candidate signals and perform division operation. We then evaluate whether accurate target area reflection signal and its adjacent area reflection signal have been correctly selected. This evaluation is based on the signal pattern after body and device motion elimination. Consequently, we output the final target waveform, effectively mitigating the influence of body and device motion.

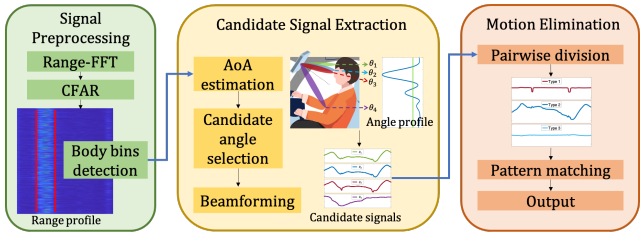

Figure 8: Overview of system design.

4.1 Signal Preprocessing

We collect signals received by the radar system. Initially, we transform the raw IF signal into a range profile using Range-FFT. As introduced in Section 2.2, due to that the distance from each body area to the radar is different, the body-reflected signals appear in multiple continuous range bins. We employ the Constant False Alarm Rate (CFAR) [36] detection approach on the range profile. The CFAR algorithm serves to identify the presence of objects within a background of noise by adaptively comparing the magnitude of adjacent range bins. Consequently, we can identify the range bins corresponding to human body reflected signals. Note that the interference from other reflections (e.g., other people moving around in the vicinity) can be avoided. This capability is offered by the fine-grained range resolution of mmWave radar, which is determined by the signal bandwidth. In our case, the signal frequency bandwidth is 4 GHz, and thus the corresponding range resolution is $\frac{c}{2B} = \frac{3\times10^8 m/s}{2\times4GHz} = 3.75\ cm$. The signals reflected from two body areas of the same person or from two different persons whose distance difference is greater than the range resolution can be separated using Range-FFT. Typically, the distance difference between the target person and other interfering persons around her/him is on the order of decimeters. Thus, the interference from these reflections is negligible.

4.2 Candidate Signal Extraction

In this module, our objective is to extract a set of candidate signals reflected from distinct areas on the human body, which will help mitigate the impact of body and device motion. As previously introduced in Section 3, our proposed approach utilizes signals reflected from two specific areas on the body to facilitate body and device motion elimination. Hence, we need to extract the reflected signals both from the target area containing the target motion, body motion and device motion, as well as from an adjacent area exhibiting the same body and device motion as the target area.

However, due to the unique physical characteristics (e.g., height and weight) of each individual and the relative position of the human body to the radar, the precise angles corresponding to the desired body parts cannot be easily obtained. For example, in eye blink detection, we cannot assume to know in advance the angle of the eye area.

To this end, we adopt a search-based method to traverse the possible angles and select candidate body parts. Specifically, in the signal processing stage, we separate the raw signal into multiple signals, each corresponding to one range bin using the method of range FFT. We then employ the Minimum Variance Distortionless Response (MVDR) [10] algorithm to acquire the angle profile of each range bin signal. It is difficult to identify the angles of the desired areas with only the magnitude information. Thus, based on the angle profile, we select as many candidate angles as possible to avoid missing important reflection signals. Note that not just the peak angles are considered. As shown in Figure 9a and 9b, we select those angles with a magnitude higher than the threshold (i.e., the mean magnitude of all angles in a particular range bin) as candidate angles (i.e., those angles in the orange rectangles). Figure 9c shows four example candidate angles and the corresponding body areas including forehead (θ_1), eyebrow (θ_2), eye (θ_3) and chest (θ_4). After that, we perform beamforming to enhance the signal strength at each candidate angle and obtain the corresponding candidate reflection signals. The enhanced signals with beamforming at these angles are shown in Figure 9d. It can be observed that the reflection signals of different body areas exhibit distinct variation patterns. We consider all candidate signals to determine the appropriate reference body part for motion cancellation.

4.3 Body and Device Motion Elimination

In this module, we eliminate body and device motion in the target area reflected signal based on candidate signals. The key practical challenge in this module is, that among all candidate signals, we need to identify the signal reflected from the target area, as well as the signal reflected from another area that exhibits the same body and device motion as the target area. Since there is no prior knowledge of where these two areas are, we perform pairwise division operation according to Equation 8 for all candidate signals. Then, based on the result of the division operation, i.e., whether the signal after division matches the pattern of target motion, we can determine whether two correct areas are selected.

We first analyze all possible types of results after the division. Theoretically, the division operation could yield three types of potential outputs. The first type of result exhibits a clean variation pattern that matches the target motion, implying successful selection of the target area and an appropriate area reflected signals. The second type indicates that the signal after division remains dominated by random body and device motions, failing to present any discernible target motion pattern. This implies that the reflected signals from

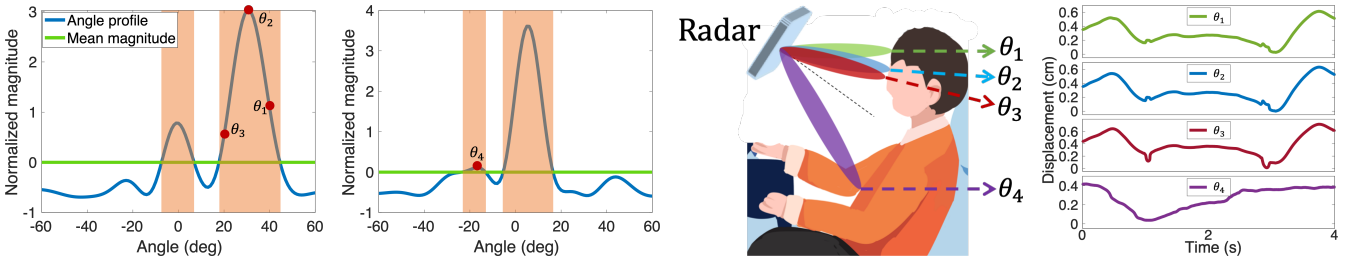

(a) Angle profile of range bin #5. (b) Angle profile of range bin #6. (c) Examples of candidate angles. (d) Examples of candidate signals.

Figure 9: Illustration of candidate signal extraction.

the target area or an appropriate area are not accurately selected. The third type of result is that the signal after division does not change with time, indicating that the two selected areas have identical motion.

To identify the signal of interest (i.e., first type) from all signals after the division operation, we initiate the process by computing the variance of each result and subsequently ranking them. Since the body and device motion typically exhibit larger displacement and randomness compared to the target motion, the third type, the first type, and the second type sequentially appear in the ranking based on variance. For the identification of the third type of signal, we compute the displacement of the signal after division. Taking respiration monitoring as an example, if the displacement change of the signal after division is less than 1 mm, we classify the signal as belonging to the third category and remove it, since respiration-induced motion exhibits displacement larger than 1 mm. Similarly, we remove certain signals of the second type based on whether their displacements exceed specific thresholds. As an example, the displacement induced by respiration typically falls within the range of 2 cm. If the signal's displacement is greater than 2 cm after division, it implies that effective cancellation of body and device motion has not been achieved. For the remaining signals, we examine whether each signal contains the target motion component in the order of variance from small to large. We apply dynamic time warping (DTW) to identify whether the signal waveform after division matches the pattern of target motion, thereby determining whether the correct areas are selected and if the motion interference is eliminated. It is worth noting that the signal pattern of each activity is unique in terms of displacement and duration. For example, nodding causes a displacement which is one order of magnitude larger than that caused by an eye blink. The pattern is also different from random noise or interference caused by other motions such as lip movements (speaking). Since we collected the signal pattern of each target movement in advance, the interference motion will not be recognized as a target motion. Meanwhile, if the reference body part has large irrelevant motions, our method would automatically select another body part as a more appropriate reference. Figure 10 shows an example of different results after the division operation. After selecting the reflected signal at θ_2 and θ_3 in Figure 9 for division, the signal fluctuation caused by eye-blinking twice can be observed (Type 1). The result of division based on the reflected signals from θ_2 and θ_4 exhibit fluctuations with non-blink pattern (Type 2), because the areas selected for division are wrong. The waveform of the third result (Type 3) hardly fluctuates with time, because the reflected signals from θ_1 and θ_2 are used for division. These two areas contain the same body and device motion, but none of them contains target motion.

We also propose a strategy to accelerate this process. It can be observed that some candidate areas exhibit the same body and device motion (e.g., the areas at θ_1 and θ_2 in Figure 9). The division of such signals yields results that do not change with time after division. Based on this observation, once we identify this type of result, one of the candidate signals is removed, thereby reducing subsequent operation overhead. Additionally, in some applications, the position of the person does not change significantly (e.g., sitting in a car). In this case, once two candidate signals are identified, the signals reflected from these two areas can be used for subsequent elimination, further reducing the computational load.

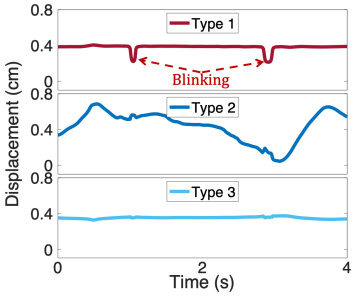

Figure 10: Illustration of three types of potential results after division.

It is worth noting that as our system relies on extracting the reflection signals from two body areas that have the same body and device motion but different target motions, the two areas are typically close to each other. Therefore, the factor that most significantly affects system performance in our design is the ability to identify and extract the reflected signals from these two areas accurately. Thus, the error in the AoA estimation and beamforming becomes the major error source of our system. If the number of antennas is not sufficient, it is difficult to separate signals from two body areas that are close to each other due to limited angle resolution.

5 IMPLEMENTATION

We implement MSense on a commercial mmWave radar, which is TI IWR1843BOOST [3]. We set the radar to operate at a starting frequency of 77 GHz with a bandwidth of 4 GHz. Two transmitting antennas and four receiving antennas are used in MIMO mode to construct equivalent eight receiving channels for angle estimation [17]. Considering that different areas of the human body are mainly distributed in the vertical direction, we place the radar vertically as shown in Figure 11. The raw intermediate frequency signals are collected by a data acquisition board, which is TI DCA1000EVM [2] and sent to a laptop through a cable. At the laptop, we set the radar parameters and control the data collection using MMWAVE-STUDIO [4]. We use a Macbook Pro with an Intel Core i7 processor and 32GB memory to process the data. The signal processing is implemented using Matlab.

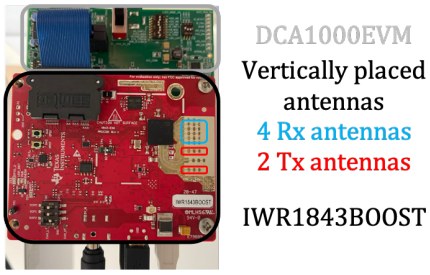

Figure 11: Hardware and device placement.

6 EVALUATION

In this section, we evaluate the performance of MSense using three real-world applications to demonstrate the effectiveness and generalization of our system: i) in-vehicle eye blink, yawn and nod detection with both body and device motion interference; ii) respiration monitoring during exercise with body motion interference; and iii) hand gesture recognition when the device is placed on a moving robot with device motion interference.

6.1 Case Study 1: In-vehicle Activity Detection Under Car Motions

In-vehicle driver sensing has wide-ranging applications, such as detection of fatigue, drunk, and distracted driving. For instance, when a driver is in the fatigue state, we can observe high-frequency nodding, yawning, and eye blinking [22, 24]. A recent work proposed to sense the driver's activities using mmWave radar [72]. However, this becomes challenging when the car is in motion. we apply MSense to realize in-vehicle driver activity detection. We ask three drivers to drive the car for a total of one hour. During the driving process, the car naturally bumps due to acceleration, braking, and turning. The drivers naturally nod, yawn, and blink during the process. Note that this experiment was conducted under the condition of ensuring the safety of drivers and pedestrians. We use the camera recording as the ground truth. Figure 13a shows the experiment scenario in the car. Figure 12 shows the precision and false positive rate of the system for detecting the three activities. The precision of detection is calculated as the ratio between the number of correctly detected activities and the total number of activities. The false positive rate indicates the proportion of wrong detection. For blinking, yawning, and nodding detection, by applying the proposed system, the precision is increased by 2.52×, 1.55×, and 1.21×, respectively. The false positive rate is decreased by 74.65%, 77.76%, and 86.29%, respectively.

Figure 13b-13d show the example of signals without and with MSense for body and device interference elimination. For fine-grained blink and yawn detection, we can see a lot of random fluctuations in the raw signal without removing body and device interference. Some of these random fluctuations have the same pattern and displacement scale as eye blink and yawn, and thus could be misidentified as targeted activities. On the other hand, when the activity does happen, there may be no fluctuation pattern corresponding to the activity. By applying MSense, we extract the reflected signals from eye-area, mouth-area, and forehead-area for body and device motion elimination. As shown in Figure 13b and 13c,

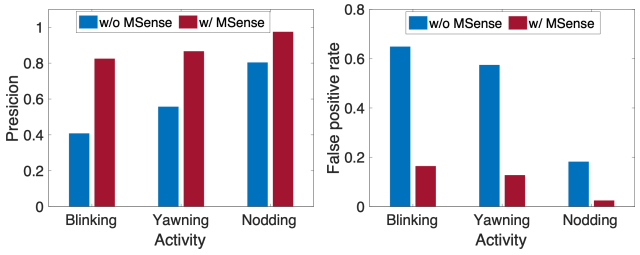

(a) Precision. **(b) False positive rate.**

Figure 12: Overall performance of eye blinking, yawning, and nodding detection.

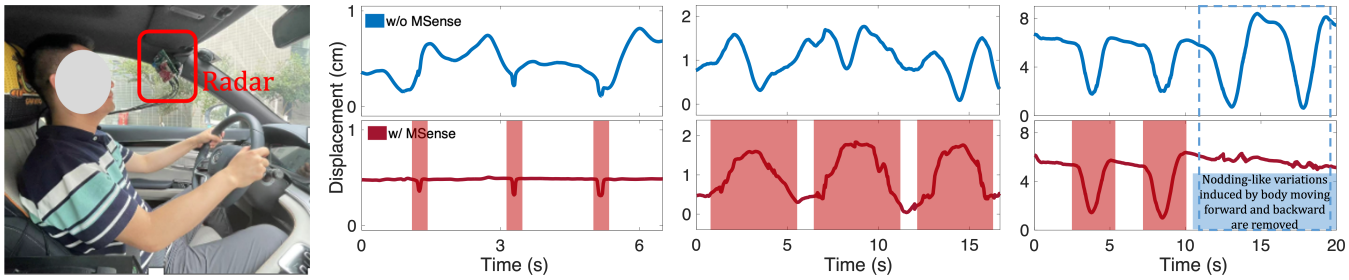

(a) Experiment scenario. (b) Eye blinking. (c) Yawning. (d) Nodding.

Figure 13: Experiment scenario of in-vehicle eye blinking, yawning, and nodding detection. Examples of signal variations before and after eliminating body and device motions.

the clear signal variation patterns induced by eye blinking and yawning can be observed after interference elimination. Nodding-induced target motion exhibits a larger scale than blinking and yawning, making it more robust against car bumps. However, we still find that when the car brakes or the person adjusts the sitting posture, the body moves, causing a motion pattern similar to nodding. For example, in Figure 13d, the fluctuation of the original signal shows four nods. Actually, the last two "nods" are caused by body motions due to car braking. MSense can reduce the false positive rate of nod detection by extracting the reflected signals from the head-area and chest-area for body motion elimination.

6.2 Case Study 2: Respiration Monitoring During Exercise Under Body Motion

6.2.1 Experiment Setup. We evaluate the performance of respiration monitoring under body motions induced by exercise in two scenarios, i.e., home and gym. As shown in Figure 14, in the home scenario, we involve four types of warm-up exercises (E1-E4). In the gym scenario, we involve four exercises with fitness equipment, which are exercise bike 1 (E5), exercise bike 2 (E6), elliptical trainer (E7), and treadmill (E8). For walking and running on the treadmill, we evaluate the system performance with five different speeds ranging from 2 km/h to 10 km/h. During experiments, the mmWave radar is fixed in front of the human body. We collect the ground truth respiration waveform using a wearable device NUL-236 [1], which monitors respiration by measuring the air pressure in the belt. We calculate the respiration rate using the auto-correlation function (ACF). The mean absolute error of respiration rate is used as the metric to verify the effectiveness of our system. We compare our system with a baseline approach Vital-Radio [7], a raw phase information-based solution without dealing with body motion. In this experiment, the system identifies the chest area and the area between the chest and neck to eliminate body motion.

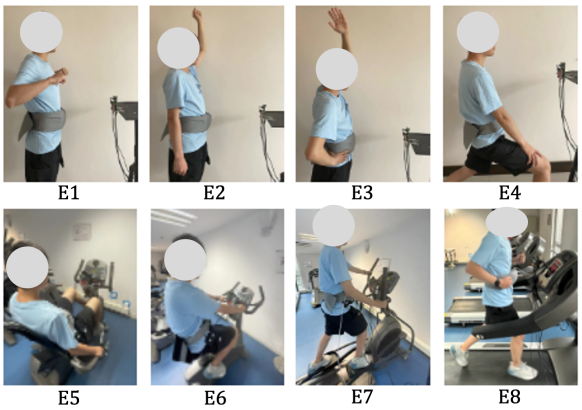

Figure 14: Different types of exercises in home and gym scenarios. The radar device is fixed in front of the human body for respiration monitoring.

6.2.2 Overall Performance. Figure 15a shows the respiration rate estimation error for different types of exercises. For all types of exercises, the respiration rate estimation errors are below 0.73 beat-per-minute (bpm). Figure 15b and 15c show an example of signal variation for exercise E3. It can be seen that the displacement estimated using the baseline method is dominated by body motion, which exhibits random variation and larger displacement than respiration. The proposed method can effectively eliminate motion interference and obtain a waveform similar to ground truth. We also test whether the system can measure changes in respiration rate on a treadmill, to demonstrate that the system can monitor breathing that is not perfectly periodic. We collect data for 100 s and change the running speed twice during this period. It can be seen that our method can estimate the change in respiration rate in a short period of time. This is because our method does not utilize periodic features to separate and recover the respiration waveform.

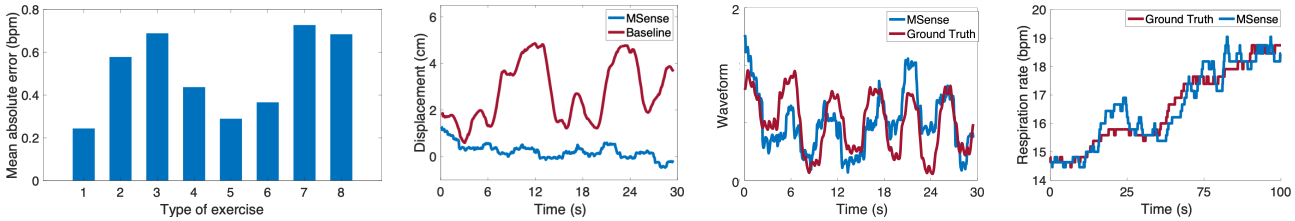

(a) Overall performance for 8 types of exercises.

(b) An example of signal variation before and after motion elimination.

(c) Comparison of recovered waveform with ground truth.

(d) Monitoring the change of respiration rate.

Figure 15: Respiration monitoring during exercise.

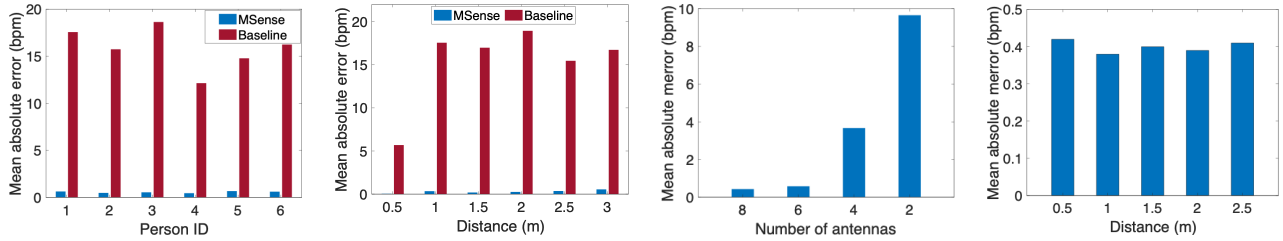

(a) Impact of target diversity.

(b) Impact of sensing distance.

(c) Impact of number of antennas.

(d) Impact of interference from other people.

Figure 16: The impact of different factors.

6.2.3 Impact of Target Diversity. We now evaluate the impact of target diversity. We recruit six subjects to test the generalization of our system across different people. As the result shown in Figure 16a, the respiration rate estimation error of our system is below 0.72 bpm for all persons, while the error of baseline methods is around 15 bpm.

6.2.4 Impact of Sensing Distance. We now evaluate the distance between the radar and the human target. The exercises in the home scenario (i.e., E1 - E4) are considered in this experiment. As shown in Figure 16b, within 3 m, our system can achieve a respiration rate error lower than 0.6 bpm. However, when the distance of human body to radar is larger than 3 m, the reflected signals from target area and the adjacent area cannot be distinguished due to the limited angle resolution, failing the proposed motion elimination scheme.

6.2.5 Impact of Number of Antennas. Our design extracts the reflection signals from two body areas that have the same body and device motions but different target motions. As discussed in Section 4.3, the capability to accurately identify and extract reflected signals from these two areas matters. This capability is dependent on the angle resolution, which is determined by the number of antennas. In our case, 8 antennas are used for AoA estimation and beamforming. In this experiment, we reduce the number of antennas from 8 to 2. Figure 16c shows an increased respiration rate estimation error as the number of antennas decreases. This is because for monitoring the respiration of an exercising person, the target area (i.e., the chest area) and the reference area (i.e., the area between the chest and the neck) are close to each other. When eight antennas are used for AoA estimation, the angle resolution is fine enough and two signals reflected from these two areas can be separated and good interference motion cancellation performance can be achieved. When the number of antennas is decreased (especially to 4 and 2), the signals reflected from the two areas can not be separated, leading to degraded system performance.

6.2.6 Impact of Interference from Other Persons. In this experiment, we evaluate the performance of target respiration monitoring during exercise when other people are moving around in the vicinity. We let another person walk near the target as an interfering person. The distance between the interfering person and the target is increased from 0.5 m to 2.5 m at a step size of 0.5 m. As shown in Figure 16d, the mean respiration rate estimation error is lower than 0.42 bpm. This is due to the fine-grained range resolution offered by mmWave radar (i.e., 3.75 cm), and we can thus separate and capture signal reflected from a small area, largely avoiding interference from other persons. This is the key

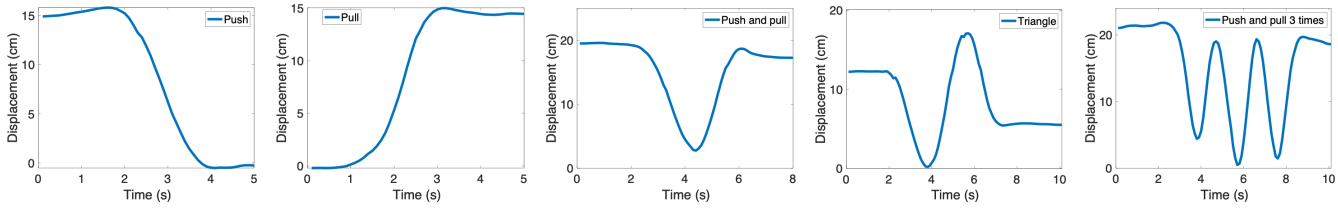

(a) Push. (b) Pull. (c) Push and pull. (d) Triangle. (e) Push and pull 3 times.

Figure 17: Examples of hand gesture waveform after motion elimination.

difference between large-bandwidth mmWave signals and narrow-bandwidth signals such as Wi-Fi.

6.3 Case Study 3: Hand Gesture Recognition with a Moving Device

Hand gesture recognition is an important application of wireless sensing. By detecting the phase change pattern caused by hand movement, the type of hand gesture can be identified. In this section, we take device motion into consideration for hand gesture recognition. As shown in Figure 18a, we place the radar on a sliding track to simulate the movement of the robot. We involve five hand gestures to evaluate the system including push, pull, push and pull, triangle, and push and pull 3 times. We let three persons perform each hand gesture ten times and the device is moving during the process. The distance between the human target and the radar is 1.5-3 m in this experiment.

We apply MSense to deal with the device motions. We adopt a classic tracking algorithm [51] to track the target. The system extracts the reflected signals from the hand-area and the abdomen-area through beamforming and then performs division to eliminate the effect of device motion. It is worth noting that the reference body area (i.e., abdomen area) also exhibits respiration-induced motion, which is different from the hand area. Fortunately, the scale of distance change induced by hand gestures is decimeter level while the scale of abdomen displacement caused by breathing is sub-centimeter level. Therefore, abdomen motion does not interfere with gesture recognition. Figure 17 shows the hand-reflected signals after device motion cancellation. Figure 18b shows the confusion matrix for gesture recognition. For various hand gestures in our experiment, the recognition accuracy is above 93%.

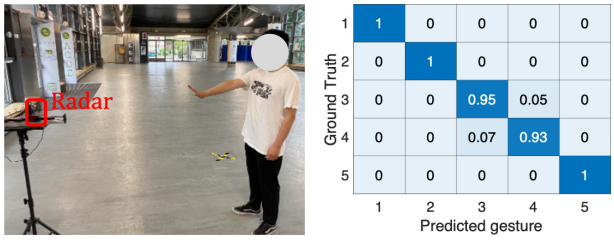

(a) Experiment scenario. (b) Confusion matrix of gesture recognition.

Figure 18: Hand gesture recognition with a moving device.

7 RELATED WORK

Wireless Sensing: In recent years, researchers have explored the use of various wireless signals for sensing including Wi-Fi [28, 43, 45], RFID [40, 67, 70], LoRa [11, 12, 52], LTE [19, 33, 38], UWB [42, 56, 63], mmWave [14, 29, 68], and acoustic signals [25, 31, 44]. Among them, mmWave radar, UWB, and acoustic signals can support fine-grained passive localization due to their large bandwidth and fine distance resolution. Meanwhile, many commercial mmWave radars have been configured with antenna array to support angle estimation and beamforming. Recently, mmWave radar has been widely used in sensing applications [9, 30, 32, 69]. However, these works assume that the human target and the radar are stationary during the sensing process. In this paper, we bring the capability of resisting body and device motions to mmWave radar sensing, enabling a variety of sensing applications in practical real-world settings.

Body and Device Motion Elimination: A recent work, Mobi^{2}Sense [65], proposes to eliminate the effect of device motion for UWB sensing. The principle behind it is that the device motion can be estimated by extracting the signal reflected from a static object in the environment. Then, the device motion component can be canceled out from the target-reflected signal. Following the same principle, RF-search [60] places mmWave radar on a drone to search for survivors by detecting respiration signals in the environment when the drone is moving. However, these approaches cannot deal with body motion because the static object reflected signal does not contain body motion information. Pi-ViMo [59] proposes a template matching method to separate vital signs from random body movements leveraging the periodic features of respiration and heartbeat activities. On the other hand, several approaches [15, 20, 55, 71] propose to utilize deep learning methods to decompose and recover vital

sign signals from signals interfered by body motions. The underlying idea behind these methods is that the periodicity or correlation of fluctuations in the temporal domain of vital sign signals differs significantly from those caused by body movements. According to the basic principle, existing methods are limited to separating and restoring periodic target motions. However, in many applications such as activity and gesture recognition, target signals can be aperiodic. Hence, previous research can not be generalized to sense aperiodic motions. In this paper, we take body and device motion elimination simultaneously into consideration for the first time. Furthermore, the proposed scheme is based on pure signal processing without a need of training or learning. Our approach can be applied to sense both periodic and aperiodic target motions.

8 DISCUSSION

Further Improve the System Performance: The key of MSense is to extract the reflected signal from the target area and another area that has the same body and device motion as the target area. The areas that are closer to the target area have a higher chance of satisfying this condition. However, a small number of antennas lead to limited angle resolution. When the target is further away from the radar, the angle difference between two specific body areas becomes smaller. Thus, the further a person is away from the radar, the more difficult it is to extract the reflected signals from two adjacent areas. If more antennas are available on radar, the working range and the sensing accuracy can both be increased. Fortunately, with the rapid progress of antenna design and manufacturing, mmWave radars are equipped with more antennas. We expect MSense to achieve better motion elimination performance in the future with more antennas.

Apply MSense to Other Wireless Sensing Systems: In addition to mmWave radar, MSense can be applied to other wireless sensing systems with fine range and angle resolutions. For narrow-band signals (e.g., Wi-Fi), since the range resolution is limited, the reflected signals from different body parts and other objects in the environment are mixed and hard to separate. However, we notice that the upcoming new Wi-Fi standard (i.e., Wi-Fi 7) brings larger signal bandwidth and more antennas, presenting the potential of applying MSense to Wi-Fi sensing.

9 CONCLUSION

In this paper, we study the effect of body and device motion interference, which is an important practical challenge in wireless sensing. We model the signal reflection from the human body considering both body and device motions. Based on the model, we eliminate the effect of body and device motions by carefully selecting the reference body area containing the same body and device motions as the target area. The proposed scheme is based on pure signal processing and can be applied to sense both periodic and aperiodic motions. We showcase three real-world sensing applications to demonstrate the effectiveness and generalization of MSense.

ACKNOWLEDGMENTS

This work is partially supported by the European Union through the Horizon EIC pathfinder challenge project SUSTAIN (No. 101071179), the Innovative Medicines Initiative 2 Joint Undertaking project IDEA-FAST (No. 853981), the National Natural Science Foundation of China (No.62172394), the Beijing Natural Science Foundation (L223034), and the Beijing Nova Program and the Youth Innovation Promotion Association, Chinese Academy of Sciences (No. 2020109).

REFERENCES

[1] 2017. Respiration Monitor Belt logger sensor NUL-236. https://neulog.com/respiration-monitor-belt/.
[2] 2023. DCA1000EVM. https://www.ti.com/tool/DCA1000EVM.
[3] 2023. IWR1843BOOST. https://www.ti.com/product/IWR1843BOOST/part-details/IWR1843BOOST.
[4] 2023. MMWAVE-STUDIO. https://www.ti.com/tool/MMWAVE-STUDIO.
[5] Fadel Adib, Chen-Yu Hsu, Hongzi Mao, Dina Katabi, and Frédo Durand. 2015. Capturing the human figure through a wall. *ACM Transactions on Graphics (TOG)* 34, 6 (2015), 1–13.
[6] Fadel Adib, Zach Kabelac, Dina Katabi, and Robert C Miller. 2014. 3D tracking via body radio reflections. In *11th USENIX Symposium on Networked Systems Design and Implementation (NSDI 14)*. 317–329.
[7] Fadel Adib, Hongzi Mao, Zachary Kabelac, Dina Katabi, and Robert C Miller. 2015. Smart homes that monitor breathing and heart rate. In *Proceedings of the 33rd annual ACM conference on human factors in computing systems*. 837–846.
[8] Sayed Saad Afzal, Atsutse Kludze, Subhajit Karmakar, Ranveer Chandra, and Yasaman Ghasempour. 2023. AgriTera: Accurate Non-Invasive Fruit Ripeness Sensing via Sub-Terahertz Wireless Signals. In *Proceedings of the 29th Annual International Conference on Mobile Computing and Networking*. 1–15.
[9] Adeel Ahmad, June Chul Roh, Dan Wang, and Aish Dubey. 2018. Vital signs monitoring of multiple people using a FMCW millimeter-wave sensor. In *2018 IEEE Radar Conference (RadarConf18)*. IEEE, 1450–1455.
[10] Jack Capon. 1969. High-resolution frequency-wavenumber spectrum analysis. *Proc. IEEE* 57, 8 (1969), 1408–1418.
[11] Zhaoxin Chang, Fusang Zhang, Jie Xiong, Junqi Ma, Beihong Jin, and Daqing Zhang. 2022. Sensor-free soil moisture sensing using lora signals. *Proceedings of the ACM on Interactive, Mobile, Wearable and Ubiquitous Technologies* 6, 2 (2022), 1–27.
[12] Lili Chen, Jie Xiong, Xiaojiang Chen, Sunghoon Ivan Lee, Kai Chen, Dianhe Han, Dingyi Fang, Zhanyong Tang, and Zheng Wang. 2019. WideSee: Towards wide-area contactless wireless sensing. In *Proceedings of the 17th Conference on Embedded Networked Sensor Systems*. 258–270.
[13] Weiyan Chen, Kai Niu, Deng Zhao, Rong Zheng, Dan Wu, Wei Wang, Leye Wang, and Daqing Zhang. 2020. Robust dynamic hand gesture interaction using LTE terminals. In *2020 19th ACM/IEEE International Conference on Information Processing in Sensor Networks (IPSN)*. IEEE,

109–120.

[14] Weiyan Chen, Hongliu Yang, Xiaoyang Bi, Rong Zheng, Fusang Zhang, Peng Bao, Zhaoxin Chang, Xujun Ma, and Daqing Zhang. 2023. Environment-aware Multi-person Tracking in Indoor Environments with MmWave Radars. *Proceedings of the ACM on Interactive, Mobile, Wearable and Ubiquitous Technologies* 7, 3 (2023), 1–29.

[15] Zhe Chen, Tianyue Zheng, Chao Cai, and Jun Luo. 2021. MoVi-Fi: Motion-robust vital signs waveform recovery via deep interpreted RF sensing. In *Proceedings of the 27th annual international conference on mobile computing and networking*. 392–405.

[16] Zhe Chen, Tianyue Zheng, and Jun Luo. 2021. Octopus: a practical and versatile wideband MIMO sensing platform. In *Proceedings of the 27th Annual International Conference on Mobile Computing and Networking*. 601–614.

[17] Reinhard Feger, Christoph Wagner, Stefan Schuster, Stefan Scheiblhofer, Herbert Jager, and Andreas Stelzer. 2009. A 77-GHz FMCW MIMO radar based on an SiGe single-chip transceiver. *IEEE Transactions on Microwave theory and Techniques* 57, 5 (2009), 1020–1035.

[18] Yuda Feng, Yaxiong Xie, Deepak Ganesan, and Jie Xiong. 2021. Lte-based pervasive sensing across indoor and outdoor. In *Proceedings of the 19th ACM Conference on Embedded Networked Sensor Systems*. 138–151.

[19] Yuda Feng, Yaxiong Xie, Deepak Ganesan, and Jie Xiong. 2022. LTE-Based Low-Cost and Low-Power Soil Moisture Sensing. In *Proceedings of the 20th ACM Conference on Embedded Networked Sensor Systems*. 421–434.

[20] Jian Gong, Xinyu Zhang, Kaixin Lin, Ju Ren, Yaoxue Zhang, and Wenxun Qiu. 2021. RF vital sign sensing under free body movement. *Proceedings of the ACM on Interactive, Mobile, Wearable and Ubiquitous Technologies* 5, 3 (2021), 1–22.

[21] Unsoo Ha, Salah Assana, and Fadel Adib. 2020. Contactless seismocardiography via deep learning radars. In *Proceedings of the 26th annual international conference on mobile computing and networking*. 1–14.

[22] Jingyang Hu, Hongbo Jiang, Daibo Liu, Zhu Xiao, Schahram Dustdar, Jiangchuan Liu, and Geyong Min. 2022. BlinkRadar: non-intrusive driver eye-blink detection with UWB radar. In *2022 IEEE 42nd International Conference on Distributed Computing Systems (ICDCS)*. IEEE, 1040–1050.

[23] Chengkun Jiang, Junchen Guo, Yuan He, Meng Jin, Shuai Li, and Yunhao Liu. 2020. mmVib: micrometer-level vibration measurement with mmwave radar. In *Proceedings of the 26th Annual International Conference on Mobile Computing and Networking*. 1–13.

[24] Sinan Kaplan, Mehmet Amac Guvensan, Ali Gokhan Yavuz, and Yasin Karalurt. 2015. Driver behavior analysis for safe driving: A survey. *IEEE Transactions on Intelligent Transportation Systems* 16, 6 (2015), 3017–3032.

[25] Dong Li, Jialin Liu, Sunghoon Ivan Lee, and Jie Xiong. 2022. Lasense: Pushing the limits of fine-grained activity sensing using acoustic signals. *Proceedings of the ACM on Interactive, Mobile, Wearable and Ubiquitous Technologies* 6, 1 (2022), 1–27.

[26] Dong Li, Jialin Liu, Sunghoon Ivan Lee, and Jie Xiong. 2022. Room-Scale Hand Gesture Recognition Using Smart Speakers. In *Proceedings of the 20th ACM Conference on Embedded Networked Sensor Systems*. 462–475.

[27] Tianhong Li, Lijie Fan, Mingmin Zhao, Yingcheng Liu, and Dina Katabi. 2019. Making the invisible visible: Action recognition through walls and occlusions. In *Proceedings of the IEEE/CVF International Conference on Computer Vision*. 872–881.

[28] Yang Li, Dan Wu, Jie Zhang, Xuhai Xu, Yaxiong Xie, Tao Gu, and Daqing Zhang. 2022. Diversense: Maximizing Wi-Fi sensing range leveraging signal diversity. *Proceedings of the ACM on Interactive, Mobile, Wearable and Ubiquitous Technologies* 6, 2 (2022), 1–28.

[29] Kun Liang, Anfu Zhou, Zhan Zhang, Hao Zhou, Huadong Ma, and Chenshu Wu. 2023. mmStress: Distilling Human Stress from Daily Activities via Contact-less Millimeter-wave Sensing. *Proceedings of the ACM on Interactive, Mobile, Wearable and Ubiquitous Technologies* 7, 3 (2023), 1–36.

[30] Haipeng Liu, Yuheng Wang, Anfu Zhou, Hanyue He, Wei Wang, Kunpeng Wang, Peilin Pan, Yixuan Lu, Liang Liu, and Huadong Ma. 2020. Real-time arm gesture recognition in smart home scenarios via millimeter wave sensing. *Proceedings of the ACM on interactive, mobile, wearable and ubiquitous technologies* 4, 4 (2020), 1–28.

[31] Wenguang Mao, Mei Wang, Wei Sun, Lili Qiu, Swadhin Pradhan, and Yi-Chao Chen. 2019. Rnn-based room scale hand motion tracking. In *The 25th Annual International Conference on Mobile Computing and Networking*. 1–16.

[32] Sameera Palipana, Dariush Salami, Luis A Leiva, and Stephan Sigg. 2021. Pantomime: Mid-air gesture recognition with sparse millimeter-wave radar point clouds. *Proceedings of the ACM on interactive, mobile, wearable and ubiquitous technologies* 5, 1 (2021), 1–27.

[33] Rui Peng, Yafei Tian, and Shengqian Han. 2023. ICI-Free Channel Estimation and Wireless Gesture Recognition Based on Cellular Signals. *IEEE Wireless Communications Letters* (2023).

[34] Qifan Pu, Sidhant Gupta, Shyamnath Gollakota, and Shwetak Patel. 2013. Whole-home gesture recognition using wireless signals. In *Proceedings of the 19th annual international conference on Mobile computing & networking*. 27–38.

[35] Kun Qian, Chenshu Wu, Yi Zhang, Guidong Zhang, Zheng Yang, and Yunhao Liu. 2018. Widar2. 0: Passive human tracking with a single Wi-Fi link. In *Proceedings of the 16th annual international conference on mobile systems, applications, and services*. 350–361.

[36] Frank C Robey, Daniel R Fuhrmann, Edward J Kelly, and Ramon Nitzberg. 1992. A CFAR adaptive matched filter detector. *IEEE Transactions on aerospace and electronic systems* 28, 1 (1992), 208–216.

[37] Xingzhe Song, Boyuan Yang, Ge Yang, Ruirong Chen, Erick Forno, Wei Chen, and Wei Gao. 2020. SpiroSonic: monitoring human lung function via acoustic sensing on commodity smartphones. In *Proceedings of the 26th Annual International Conference on Mobile Computing and Networking*. 1–14.

[38] Guanlong Teng, Feng Hong, Yue Xu, Jianbo Qi, Ruobing Jiang, Chao Liu, and Zhongwen Guo. 2020. MobiFit: Contactless Fitness Assistant for Freehand Exercises Using Just One Cellular Signal Receiver. In *2020 16th International Conference on Mobility, Sensing and Networking (MSN)*. IEEE, 299–306.

[39] Anran Wang, Jacob E Sunshine, and Shyamnath Gollakota. 2019. Contactless infant monitoring using white noise. In *The 25th Annual International Conference on Mobile Computing and Networking*. 1–16.

[40] Chuyu Wang, Jian Liu, Yingying Chen, Hongbo Liu, Lei Xie, Wei Wang, Bingbing He, and Sanglu Lu. 2018. Multi-touch in the air: Device-free finger tracking and gesture recognition via cots rfid. In *IEEE INFOCOM 2018-IEEE conference on computer communications*. IEEE, 1691–1699.

[41] Hao Wang, Daqing Zhang, Junyi Ma, Yasha Wang, Yuxiang Wang, Dan Wu, Tao Gu, and Bing Xie. 2016. Human respiration detection with commodity WiFi devices: Do user location and body orientation matter?. In *Proceedings of the 2016 ACM international joint conference on pervasive and ubiquitous computing*. 25–36.

[42] Pei Wang, Xujun Ma, Rong Zheng, Luan Chen, Xiaolin Zhang, Djamal Zeghlache, and Daqing Zhang. 2023. SlpRoF: Improving the Temporal Coverage and Robustness of RF-based Vital Sign Monitoring during Sleep. *IEEE Transactions on Mobile Computing* (2023).

[43] Wei Wang, Alex X Liu, Muhammad Shahzad, Kang Ling, and Sanglu Lu. 2015. Understanding and modeling of wifi signal based human activity recognition. In *Proceedings of the 21st annual international conference on mobile computing and networking*. 65–76.

[44] Wei Wang, Alex X Liu, and Ke Sun. 2016. Device-free gesture tracking using acoustic signals. In *Proceedings of the 22nd Annual International Conference on Mobile Computing and Networking*. 82–94.

[45] Xuanzhi Wang, Kai Niu, Anlan Yu, Jie Xiong, Zhiyun Yao, Junzhe Wang, Wenwei Li, and Daqing Zhang. 2023. WiMeasure: Millimeter-level Object Size Measurement with Commodity WiFi Devices. *Proceedings of the ACM on Interactive, Mobile, Wearable and Ubiquitous Technologies* 7, 2 (2023), 1–26.

[46] Yanwen Wang, Jiaxing Shen, and Yuanqing Zheng. 2020. Push the limit of acoustic gesture recognition. *IEEE Transactions on Mobile Computing* 21, 5 (2020), 1798–1811.

[47] Zhu Wang, Yifan Guo, Zhihui Ren, Wenchao Song, Zhuo Sun, Chao Chen, Bin Guo, and Zhiwen Yu. 2024. LiqDetector: Enabling Container-Independent Liquid Detection with mmWave Signals Based on a Dual-Reflection Model. *Proceedings of the ACM on Interactive, Mobile, Wearable and Ubiquitous Technologies* 7, 4 (2024), 1–24.

[48] Zhi Wang, Beihong Jin, Siheng Li, Fusang Zhang, and Wenbo Zhang. 2023. ECG-grained Cardiac Monitoring Using UWB Signals. *Proceedings of the ACM on Interactive, Mobile, Wearable and Ubiquitous Technologies* 6, 4 (2023), 1–25.

[49] Teng Wei and Xinyu Zhang. 2015. mtrack: High-precision passive tracking using millimeter wave radios. In *Proceedings of the 21st Annual International Conference on Mobile Computing and Networking*. 117–129.

[50] Chenhao Wu, Xuan Huang, Jun Huang, and Guoliang Xing. 2023. Enabling Ubiquitous WiFi Sensing with Beamforming Reports. In *Proceedings of the ACM SIGCOMM 2023 Conference*. 20–32.

[51] Chenshu Wu, Feng Zhang, Beibei Wang, and KJ Ray Liu. 2020. mmTrack: Passive multi-person localization using commodity millimeter wave radio. In *IEEE INFOCOM 2020-IEEE Conference on Computer Communications*. IEEE, 2400–2409.

[52] Binbin Xie, Minhao Cui, Deepak Ganesan, Xiangru Chen, and Jie Xiong. 2023. Boosting the Long Range Sensing Potential of LoRa. In *Proceedings of the 21st Annual International Conference on Mobile Systems, Applications and Services*. 177–190.

[53] Binbin Xie, Jie Xiong, Xiaojiang Chen, and Dingyi Fang. 2020. Exploring commodity rfid for contactless sub-millimeter vibration sensing. In *Proceedings of the 18th Conference on Embedded Networked Sensor Systems*. 15–27.

[54] Jie Xiong and Kyle Jamieson. 2013. ArrayTrack: A Fine-Grained indoor location system. In *10th USENIX Symposium on Networked Systems Design and Implementation (NSDI 13)*. 71–84.

[55] Xiangyu Xu, Jiadi Yu, Yingying Chen, Yanmin Zhu, Linghe Kong, and Minglu Li. 2019. Breathlistener: Fine-grained breathing monitoring in driving environments utilizing acoustic signals. In *Proceedings of the 17th Annual International Conference on Mobile Systems, Applications, and Services*. 54–66.

[56] Yanni Yang, Jiannong Cao, Xiulong Liu, and Xuefeng Liu. 2019. Multi-breath: Separate respiration monitoring for multiple persons with UWB radar. In *2019 IEEE 43rd Annual Computer Software and Applications Conference (COMPSAC)*, Vol. 1. IEEE, 840–849.

[57] Yanni Yang, Huafeng Xu, Qianyi Chen, Jiannong Cao, and Yanwen Wang. 2023. Multi-Vib: Precise Multi-point Vibration Monitoring Using mmWave Radar. *Proceedings of the ACM on Interactive, Mobile, Wearable and Ubiquitous Technologies* 6, 4 (2023), 1–26.

[58] Shang Zeng, Haoran Wan, Shuyu Shi, and Wei Wang. 2023. mSilent: Towards General Corpus Silent Speech Recognition Using COTS mmWave Radar. *Proceedings of the ACM on Interactive, Mobile, Wearable and Ubiquitous Technologies* 7, 1 (2023), 1–28.

[59] Bo Zhang, Boyu Jiang, Rong Zheng, Xiaoping Zhang, Jun Li, and Qiang Xu. 2023. Pi-ViMo: Physiology-inspired Robust Vital Sign Monitoring using mmWave Radars. *ACM Transactions on Internet of Things* 4, 2 (2023), 1–27.

[60] Bin-Bin Zhang, Dongheng Zhang, Ruiyuan Song, Binquan Wang, Yang Hu, and Yan Chen. 2023. RF-Search: Searching Unconscious Victim in Smoke Scenes with RF-enabled Drone. In *Proceedings of the 29th Annual International Conference on Mobile Computing and Networking*. 1–15.

[61] Duo Zhang, Xusheng Zhang, Shengjie Li, Yaxiong Xie, Yang Li, Xuanzhi Wang, and Daqing Zhang. 2023. LT-Fall: The Design and Implementation of a Life-threatening Fall Detection and Alarming System. *Proceedings of the ACM on Interactive, Mobile, Wearable and Ubiquitous Technologies* 7, 1 (2023), 1–24.

[62] Fusang Zhang, Zhaoxin Chang, Kai Niu, Jie Xiong, Beihong Jin, Qin Lv, and Daqing Zhang. 2020. Exploring lora for long-range through-wall sensing. *Proceedings of the ACM on Interactive, Mobile, Wearable and Ubiquitous Technologies* 4, 2 (2020), 1–27.

[63] Fusang Zhang, Zhaoxin Chang, Jie Xiong, Junqi Ma, Jiazhi Ni, Wenbo Zhang, Beihong Jin, and Daqing Zhang. 2023. Embracing Consumer-level UWB-equipped Devices for Fine-grained Wireless Sensing. *Proceedings of the ACM on Interactive, Mobile, Wearable and Ubiquitous Technologies* 6, 4 (2023), 1–27.

[64] Fusang Zhang, Zhaoxin Chang, Jie Xiong, Rong Zheng, Junqi Ma, Kai Niu, Beihong Jin, and Daqing Zhang. 2021. Unlocking the beamforming potential of LoRa for long-range multi-target respiration sensing. *Proceedings of the ACM on Interactive, Mobile, Wearable and Ubiquitous Technologies* 5, 2 (2021), 1–25.

[65] Fusang Zhang, Jie Xiong, Zhaoxin Chang, Junqi Ma, and Daqing Zhang. 2022. Mobi2Sense: empowering wireless sensing with mobility. In *Proceedings of the 28th Annual International Conference on Mobile Computing And Networking*. 268–281.

[66] Shigeng Zhang, Xuan Liu, Yangyang Liu, Bo Ding, Song Guo, and Jianxin Wang. 2020. Accurate respiration monitoring for mobile users with commercial RFID devices. *IEEE Journal on Selected Areas in Communications* 39, 2 (2020), 513–525.

[67] Shigeng Zhang, Zijing Ma, Kaixuan Lu, Xuan Liu, Jia Liu, Song Guo, Albert Y Zomaya, Jian Zhang, and Jianxin Wang. 2022. Hearme: Accurate and real-time lip reading based on commercial rfid devices. *IEEE Transactions on Mobile Computing* (2022).

[68] Xusheng Zhang, Duo Zhang, Yaxiong Xie, Dan Wu, Yang Li, and Daqing Zhang. 2024. Waffle: A Waterproof mmWave-based Human Sensing System inside Bathrooms with Running Water. *Proceedings of the ACM on Interactive, Mobile, Wearable and Ubiquitous Technologies* 7, 4 (2024), 1–29.

[69] Xi Zhang, Yu Zhang, Zhenguo Shi, and Tao Gu. 2023. mmFER: Millimetre-wave Radar based Facial Expression Recognition for Multimedia IoT Applications. In *Proceedings of the 29th Annual International Conference on Mobile Computing and Networking*. 1–15.

[70] Cui Zhao, Zhenjiang Li, Han Ding, Ge Wang, Wei Xi, and Jizhong Zhao. 2022. RF-Wise: Pushing the Limit of RFID-based Sensing. In *IEEE INFOCOM 2022-IEEE Conference on Computer Communications*. IEEE, 1779–1788.

[71] Tianyue Zheng, Zhe Chen, Shujie Zhang, Chao Cai, and Jun Luo. 2021. More-fi: Motion-robust and fine-grained respiration monitoring via deep-learning uwb radar. In *Proceedings of the 19th ACM conference on embedded networked sensor systems*. 111–124.

[72] Juncen Zhu, Jiannong Cao, Yanni Yang, Wei Ren, and Huizi Han. 2023. mmDrive: Fine-Grained Fatigue Driving Detection Using mmWave Radar. *ACM Transactions on Internet of Things* (2023).